Late Pleistocene to Holocene slip rates for the Gurvan Bulag thrust fault (Gobi-Altay, Mongolia) estimated with ^{10}Be dates

J.-F. Ritz,[1] D. Bourlès,[2] E. T. Brown,[3] S. Carretier,[4] J. Chéry,[1] B. Enhtuvshin,[5] P. Galsan,[5] R. C. Finkel,[6] T. C. Hanks,[7] K. J. Kendrick,[8] H. Philip,[1] G. Raisbeck,[9] A. Schlupp,[10] D. P. Schwartz,[7] and F. Yiou[9]

Received 30 March 2001; revised 3 June 2002; accepted 28 August 2002; published 20 March 2003.

[1] We surveyed morphotectonic markers along the central part of the Gurvan Bulag thrust, a fault that ruptured with the Bogd fault during the Gobi-Altay earthquake (1957, *M* 8.3), to document climatic and tectonic processes along the fault for the late Pleistocene-Holocene period. The markers were dated using ^{10}Be produced in situ. Two major periods of alluviation ended at 131 ± 20 and 16 ± 4.8 ka. These appear to be contemporaneous with global climatic changes at the terminations of marine isotope stages (MIS) 6 and 2. The vertical slip rates, determined from offset measurements and surfaces ages, are 0.14 ± 0.03 mm/yr over the late Pleistocene-Holocene and between 0.44 ± 0.11 and 1.05 ± 0.25 mm/yr since the end of the late Pleistocene. The higher of these slip rates for the last ~16 kyr is consistent with paleoseismic investigations along the fault [*Prentice et al.*, 2002], and suggests that, at the end of late Pleistocene, the fault evolved from quiescence to having recurrence intervals of 4.0 ± 1.2 kyr for surface ruptures with ~4 m vertical offset (similar to that of 1957). The inferred recurrence interval is comparable to that of the Bogd fault (3.7 ± 1.3 kyr) suggesting that the two faults may have ruptured together also earlier during the last ~16 kyr. *INDEX TERMS:* 7221 Seismology: Paleoseismology; 1208 Geodesy and Gravity: Crustal movements—intraplate (8110); 1824 Hydrology: Geomorphology (1625); 7230 Seismology: Seismicity and seismotectonics; 8107 Tectonophysics: Continental neotectonics; *KEYWORDS:* Late Pleistocene, Holocene, thrust fault, slip rate, 10Be dating, Mongolia

Citation: Ritz, J.-F., et al., Late Pleistocene to Holocene slip rates for the Gurvan Bulag thrust fault (Gobi-Altay, Mongolia) estimated with ^{10}Be dates, *J. Geophys. Res.*, *108*(B3), 2162, doi:10.1029/2001JB000553, 2003.

1. Introduction and Tectonic Setting

[2] Recent advances in paleoseismology have demonstrated the importance of studying active faulting over several seismic cycles [e.g., *McCalpin*, 1996; *Yeats and Prentice*, 1996]. Even in regions where strain rates are high (i.e., interplate settings), instrumental and historical records of seismicity are barely representative of a complete seismic cycle, emphasizing the importance of paleoseismic studies. Moreover, some examples of long-term analyses of seismic activity have shown that periods of activity can alternate with periods of quiescence along a single fault or a group of faults [e.g., *Sieh et al.*, 1989; *Grant and Sieh*, 1994; *Marco et al.*, 1996; *Xiwei and Qidong*, 1996; *Khair et al.*, 2000]. This emphasizes the need for understanding the behavior of faults over longer periods of geologic history.

[3] In this paper, we use in situ-produced ^{10}Be to determine the rate of late Quaternary vertical slip along the Gurvan Bulag fault (Figures 1–3). The Gurvan Bulag fault is a 23 km long thrust that ruptured most recently in 1957, simultaneously with the Bogd strike-slip fault during one of the strongest seismic event (*M* 8.3) to have occurred in continental interiors during the last century [*Florensov and Solonenko*, 1965; *Molnar and Qidong*, 1984; *Baljinnyam et al.*, 1993; *Kurushin et al.*, 1997]. Determining the vertical slip rate along the Gurvan Bulag thrust fault over a long time period will permit examination of interaction between the Bogd and Gurvan Bulag faults, notably whether the two faults ruptured together in the past as well.

[4] Morphological analysis along the Bogd fault provides evidence of cumulative displacements, such as the offset of streams, ridges, or alluvial fans. This has allowed estimation of the late Quaternary slip rate along the Bogd fault. At Noyan Uul, along the main strike-slip segment of the Bogd fault, *Ritz et al.* [1995] estimated a maximum horizontal slip

[1]Laboratoire de Géophysique, Tectonique et Sédimentologie, UMR 5573 Université Montpellier II, Montpellier, France.
[2]CEREGE, Europole Méditerranéen de l'Arbois, Aix-en-Provence, France.
[3]Large Lakes Observatory, University of Minnesota, Duluth, Minnesota, USA.
[4]BRGM/ARN3, Orleans, France.
[5]Centre of Informatic and Remote Sensing, Mongolian Academy of Sciences, Ulaanbaatar, Mongolia.
[6]Lawrence Livermore National Laboratory, University of California, Livermore, California, USA.
[7]U.S. Geological Survey, Menlo Park, California, USA.
[8]U.S. Geological Survey, Pasadena, California, USA.
[9]Centre de Spectrométrie Nucléaire et de Spectrométrie de Masse, Orsay, France.
[10]LDG-CEA, Bruyères-le-Chatel, France.

0148-0227/03/2001JB000553$09.00

Figure 1. Photograph of the central part of Gurvan Bulag active thrusting ridge ("foreberg") at the southern foothills of Ih Bogd massif, taken from a distance of 5 km.

rate of 1.2 mm/yr from an offset alluvial fan dated by cosmogenic ^{10}Be produced in situ (Figure 2). This rate suggests recurrence intervals on the order of 5 kyr for surface rupture similar to that of 1957. Preliminary interpretation of ^{10}Be dates of offset morphotectonic markers along the Gurvan Bulag thrust fault suggested variations of vertical slip rate through time [*Ritz et al.*, 1997], and therefore a possible episodic behavior of the faulting process, which has not been proposed for the Bogd fault. Nevertheless, such episodic behavior has been suggested for other secondary thrust faults associated with the Bogd fault system [*Owen et al.*, 1999].

[5] The topography of the region appears tightly associated with geometry, kinematics, and distribution of ruptures (Figure 2b). Along the Ih Bogd and Baga Bogd massifs, the left lateral slip is associated with a vertical reverse component. The two massifs of Ih Bogd and Baga Bogd are bounded by oblique reverse faults along their northern flanks and pure reverse faults along their southern flanks. They can be considered as rigid pop-up structures resulting from transpressional deformations within restraining bends along the Bogd strike-slip fault [*Kurushin et al.*, 1997; *Cunningham et al.*, 1996, 1997]. The flat summit plateau of the Ih Bogd massif (Figure 3c), an elevated remnant of an old erosional surface [*Florensov and Solonenko*, 1965; *Baljinnyam et al.*, 1993] suggests that the bounding faults have the same long-term slip rate. *Hanks et al.* [1997] reported a ~0.1 mm/yr vertical slip rate for the past 100 ka along a thrust fault segment to the north of the Ih Bogd massif, southeast of Dalan Türüü foreberg (Figure 2b). The massif rises more than 2000 m above the E-W trending Valley-of-Lakes to the north, and about 1500 m above its southern piedmont. Determination of the long-term uplift rate along the Gurvan Bulag fault should permit evaluation of the uplift history of the Ih Bogd massif.

[6] The mountain ranges of northern Central Asia, the Altay, the Gobi-Altay, and the Sayan mountains, represent the northernmost compressional active belts in Asia [*Molnar and Tapponnier*, 1975; *Tapponnier and Molnar*, 1979] (Figure 2a). Western Mongolia was the site of four $M \geq 8$ earthquakes during the last century, and thus may be considered among the most active intracontinental regions [e.g., *Baljinnyam et al.*, 1993; *Schlupp*, 1996; *Cunningham et al.*, 1996; *Bayasgalan*, 1999].

[7] In 1957, the most recent of these, the Gobi-Altay earthquake, ruptured the eastern part of the Valley-of-Lakes fault, an ancient Paleozoic structure that was reactivated during the Cenozoic era [*Florensov and Solonenko*, 1965]. The following year, a Mongolian-Russian expedition to the epicentral zone provided an outstanding description of ground surface effects of the earthquake [*Florensov and Solonenko*, 1965]. Recently, *Baljinnyam et al.* [1993] revisited some of the piercing points of the surface breaks and *Kurushin et al.* [1997] furnished an updated and thorough description of the whole rupture area. The main rupture of more than 260 km of left lateral strike-slip occurred along the Bogd fault, to the north of the Ih Bogd (3957 m) and Baga Bogd (3590 m) massifs (Figure 2b). The average horizontal displacement was between 3 and 4 m with a maximum section of offsets up to 5–7 m [*Kurushin et al.*, 1997]. An additional 100 km of reverse faulting, distributed

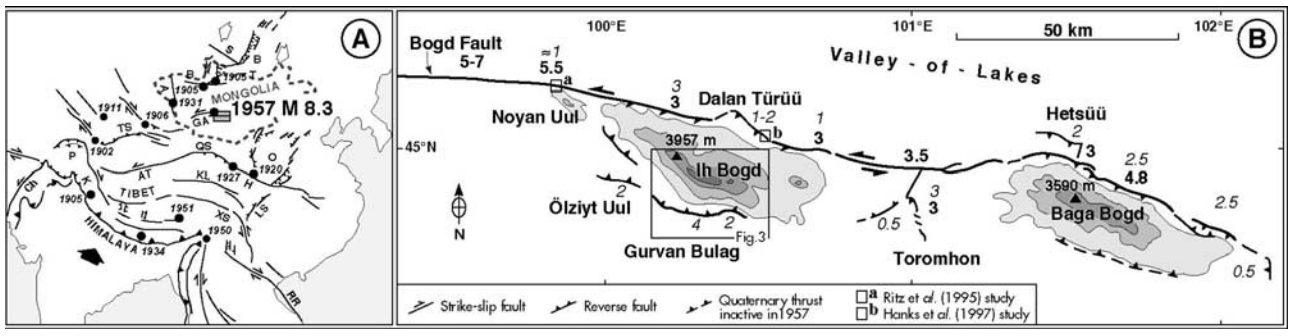

Figure 2. (a) Simplified map of Quaternary faults (symbols noted subsequently) in Central Asia and $M \geq 8$ earthquakes (solid dots) recorded during the past century [modified after *Molnar and Qidong*, 1984]: B, Baikal; S, Sayan; T, Tsetserleg; B, Bolnay; A, Altay; GA, Gobi-Altay; TS, Tien Shan; P, Pamir; AT, Altyn Tagh; QS, Qilian Shan; O, Ordos; H, Haiyuan; KL, Kun Lun; LS, Lungmen Shan; XS, Xian Shui; RR, Red River; K, Karakorum; Ch, Chaman. (b) Sketch map of the 1957 Gobi-Altay rupture. Bold and italic numbers indicate horizontal and vertical displacements, respectively, in meters [data from *Kurushin et al.*, 1997].

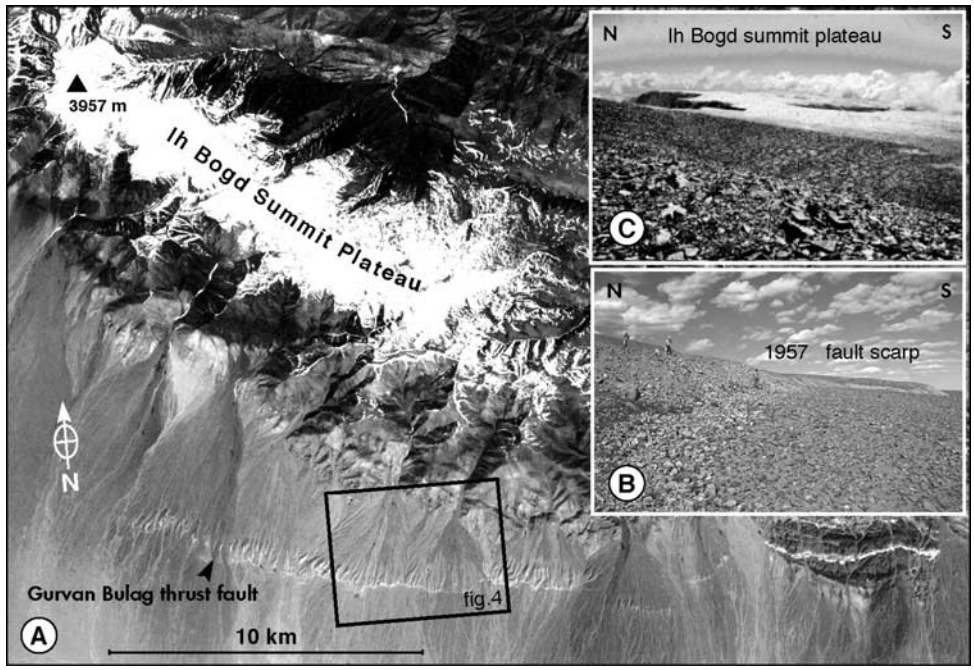

Figure 3. (a) Panchromatic SPOT image of Ih Bogd massif covered by a thin snow cap, showing the 23 km long Gurvan Bulag foreberg to the South of the massif. (b) The 1957 fault scarp about 4 m high in the central part of Gurvan Bulag thrust fault. (c) View toward the East of Ih Bogd summit surface (picture taken near the 3957 m altitude marker in Figure 3a).

on five secondary segments, ruptured simultaneously with the Bogd fault during the 1957 earthquake (Ölziyt, Gurvan Bulag, Toromhon, Dalaan Türüü, and Hetsüü; Figure 2b) [*Florensov and Solonenko*, 1965; *Kurushin et al.*, 1997]. These fault segments correspond mainly to thrust faults found at the base of ridges and low hills or "forebergs" [*Florensov and Solonenko*, 1965; *Kurushin et al.*, 1997; *Owen et al.*, 1999; *Bayasgalan et al.*, 1999b], which are shortening structures associated with the main Bogd strike-slip fault. The foreberg associated with the Gurvan Bulag fault, to the south of the Ih Bogd massif, is the major field area for the present study.

[8] The morphology of the Gurvan Bulag foreberg is the result of the interactions between tectonics (vertical offset) and fan dynamics (erosion or deposition) [*Bayasgalan et al.*, 1999a; *Carretier et al.*, 2002]. Flat, active surfaces are generally directly downstream of drainage basins where erosional and depositional rates are at a maximum, whereas hills are found in areas where deposition rates are lower, typically at the lateral margins of the fans (Figures 3 and 4). The foreberg is thus a system of inset surfaces that show clear cumulative vertical slips. These surfaces, containing quartz-rich boulders, offer the possibility to evaluate the vertical slip rate of the Gurvan Bulag thrust fault during the late Quaternary, using cosmic ray exposure dating.

2. Morphotectonic Analysis

2.1. Analysis of Aerial Photographs

[9] This study focused on two fans cut by the central part of the Gurvan Bulag thrust fault (Figure 3) and where the 1957 vertical displacements were the largest [*Kurushin et al.*, 1997]. Analysis of 1:35,000 scale Soviet-Mongolian aerial photographs taken of these fans in 1958, allowed us to identify three main alluvial markers from their relative elevations (Figure 4). S1 corresponds to upper, old eroded surfaces found within the hanging wall in a band of 1–1.5 km width uphill from the fault scarp. They result either from fold thrusting or represent elevated remnants of planar abrasive or depositional surfaces. S2 is an intermediate alluvial surface inset in S1 and is found in large patches extending on both sides of the fault. Within it, we distinguished S2a from S2b according to differences in stream system morphology. S2a is found mainly in the hanging wall block and shows a low-density, strongly incised stream pattern. S2b is found mainly within the footwall block and has a dense superficial stream system converging downstream, which we interpret as the result of localized erosional processes (e.g., diffuse sheet wash, rilling). S3 is the youngest depositional surface, extending from the apex of the cones to the Gurvan Bulag foreberg, and appears to be inset in S2. In the western fan (Figure 4) as it approaches the fault zone, S3 overlies surface S2 and then dissipates before reaching the fault scarp, except maybe along the main, narrow stream channel. This termination of S3 deposits above the fault scarp has also been described further east at Gurvan Bulag [*Carretier et al.*, 2002]. However, it is not observed within the eastern fan in our study area, where S3 is more deeply inset within the two older surfaces and crosses the fault scarp in broad channels (Figure 4).

[10] In addition to these three main alluvial surfaces, the aerial photographs also enabled us to define additional features present only within the western fan: S4 corresponds to gullies cut in alluvial surfaces near the fault scarp, and C are local cones which are found in the footwall in front of S4 gullies. We interpret these features as local debris cones

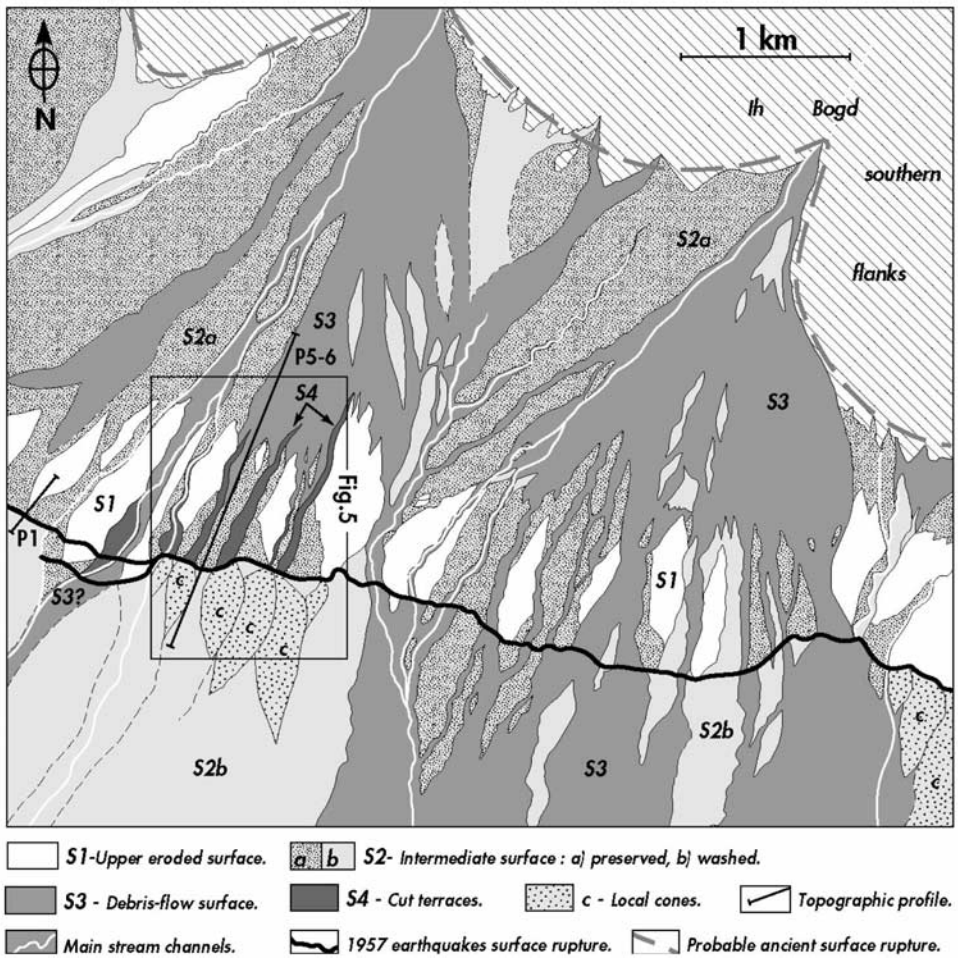

Figure 4. Simplified morphological map of inset surfaces observed within two fans affected by the Gurvan Bulag rupture (see Figure 3a for location).

that accumulated at the toeslope of the fault scarp contemporaneously with the incision of S4 gullies into older hanging wall alluvial surfaces.

2.2. Fieldwork

[11] We focused our fieldwork within the western fan, where the 1957 fault displacements, as well as the cumulative deformation, appeared largest, and where the surfaces and their associated deposits seemed to be the broadest and the best preserved (Figure 5). Field observations of the surfaces defined through the use of aerial photographs permitted more detailed morphological descriptions. S1, the high surfaces, have the morphology of uplifted N-S elongated hills. Flat tops are still observed in some places, but in most cases tops are rounded (Figure 6). These surfaces contain deeply weathered granite boulders totally engulfed in more finer material. S2 is well inset within S1 and shows a planar morphology with large boulders (1 m in average) almost totally encased in the surface. Some rare, weathered, and often fractured boulders are still elevated on the surface, their lower parts encased in finer deposits (Figures 7 and 10). S3 appears as a broad debris flow characterized by a dense boulder field (Figures 6b and 7). This debris flow contains well-preserved large granite boulders (up to 3 m, 1 m in average) that are embedded in a finer matrix. Many of the boulders have dark desert varnish and some of these have petroglyphs, reportedly 3000-yr-old [*Florensov and Solonenko*, 1965]. At the studied site, S3 covers surface S2, but terminates before reaching the fault scarp (Figures 6b and 7). S4, the most recent morphologic marker, is present in 50 m wide gullies near the fault, and corresponds to cut terraces incised into older fill terrace material. Their transverse profile defines a concave surface covered by soil containing cobbles (Figures 6 and 8). Close to the fault, these gullies are more or less incised along the stream channels due to the post-1957 regressive erosion along intermittent streams. In the field, we also observed a local debris flow, called S5, inset into one of the S4 gullies (Figures 5b and 14). This recent debris flow unit was offset during the 1957 earthquake and shows $\sim$2.5 m high, sharp, vertical risers due to rapid stream incision following to the 1957 earthquake.

2.3. Measurement of Offsets

2.3.1. Offsets Associated With 1957 and Penultimate Earthquakes

[12] From the described features, we attempted to estimate the amount of the 1957 offsets and of cumulative vertical offsets along this portion of the Gurvan Bulag thrust fault. We surveyed the morphology of the surfaces by

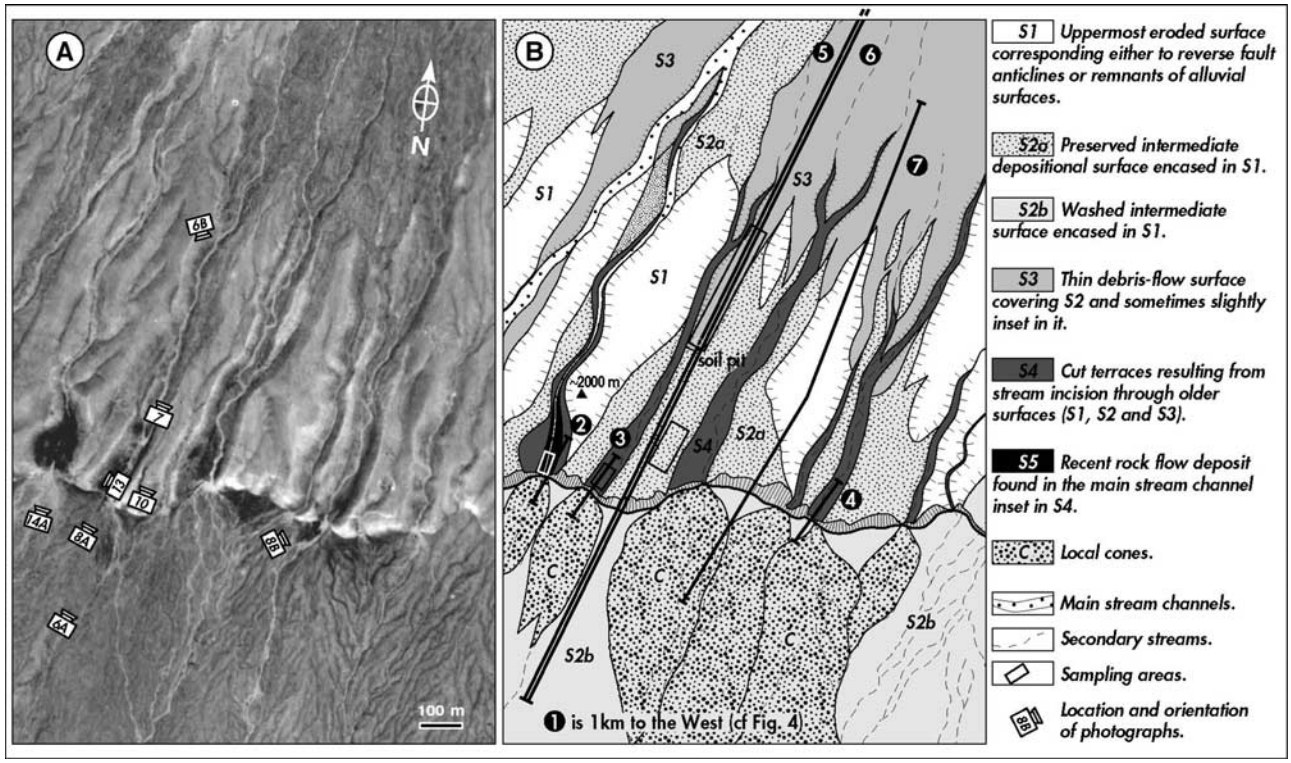

Figure 5. (a) Aerial photograph of the Gurvan Bulag thrust fault study site (see Figure 4 for location). (b) Corresponding detailed morphotectonic map drawn from stereoscopic analysis and field observations.

measuring cross profiles with kinematic GPS using two Ashtech receivers (Figure 9a). One was used as a base, its antenna fixed on a tripod downstream from the fault scarp; the other one was mobile, its antenna attached to a hand-carried pole. Both receivers recorded positioning data (from at least four satellites) at intervals of 3, 5, or 10 s depending on the length of profiles and the need for topographic detail. After the surveys, positioning data were processed with GPPS and KINSVY Ashtech software. Remeasurements of starting points for each profile indicated horizontal and vertical uncertainties on the order of 1 cm. We measured seven profiles across the different surfaces (see Figures 4 and 5). Results are shown in Figure 9b. Vertical displacements and associated uncertainties were calculated from the profiles using mathematical parameterizations developed by *Hanks et al.* [1984] from the work of *Bucknam and Anderson* [1979].

[13] Profile 1 is perpendicular to the fault and follows the crest of a ridge contiguous with surface S1 (Figure 4). The slope morphology associated with the 1957 scarp along this profile displays a typical single event scarp degradation profile. It is characterized by a straight, steep linear backslope, with a concave toeslope and convex shoulder. Estimation of the 1957 vertical separation from this profile is 4.0 ± 0.3 m.

[14] Profiles 2, 3, and 4, also perpendicular to the fault, cross surfaces S4 and simple interpretation suggests larger vertical slip values: 5.6 ± 0.2, 7.8 ± 0.4, and 6.0 ± 0.5 m, respectively. However, the shapes of profiles 2 and 3 show complex slope morphology suggesting that more than one event is recorded in the scarp. The lower parts of both profiles are linear and we interpret them as the gravity-controlled face associated with the 1957 event [*Carretier et al.*, 2002]. Assuming that the height of these faces represents an upper limit for the 1957 vertical offset, we determined values of 4.0 ± 0.2 and 4.5 ± 0.4 m along profiles 2 and 3, respectively. Upper parts of both profiles display beveled surfaces with mounds and hollows that we interpret as degraded preexisting scarps (see Figure 9b). If we interpret the beveled parts of profiles as degraded scarps from a single prior event, the minimum vertical offset associated with this penultimate event is 1.6 ± 0.2 and 3.3 ± 0.4 m, respectively. Note that we do not observe the symmetrical change in slope downstream the 1957 gravity-controlled faces, corresponding to the slope front filled due to the degradation of the penultimate scarp. There are two possible explanations for this: either the debris were removed further downstream or, as proposed by *Carretier et al.* [2002], the 1957 fault rupture stepped forward at the bottom the penultimate degraded scarp.

[15] Profile 4 (Figures 8b and 9b) corresponds to site 44 of *Kurushin et al.* [1997, their Figure A44b] in which the 1957 vertical offset is estimated at 5.2 ± 0.5 m. Our profile displays an apparent symmetry that might be interpreted as a single event scarp with a height of 6.0 ± 0.5 m. Nevertheless, the fact that profile 4 crosscuts (400 m to the east) the same fault scarp as profiles 2 and 3 which have evidence for two events, suggests that the scarp at profile 4 also is the result of multiple events. We believe that the apparent straight, linear face does not represent the 1957 fault scarp, but was formed by recent gravitational collapse of the cumulative frontal part of the scarp at this site. Such collapse would have removed the preexisting topography associated with the penultimate event. This precludes the

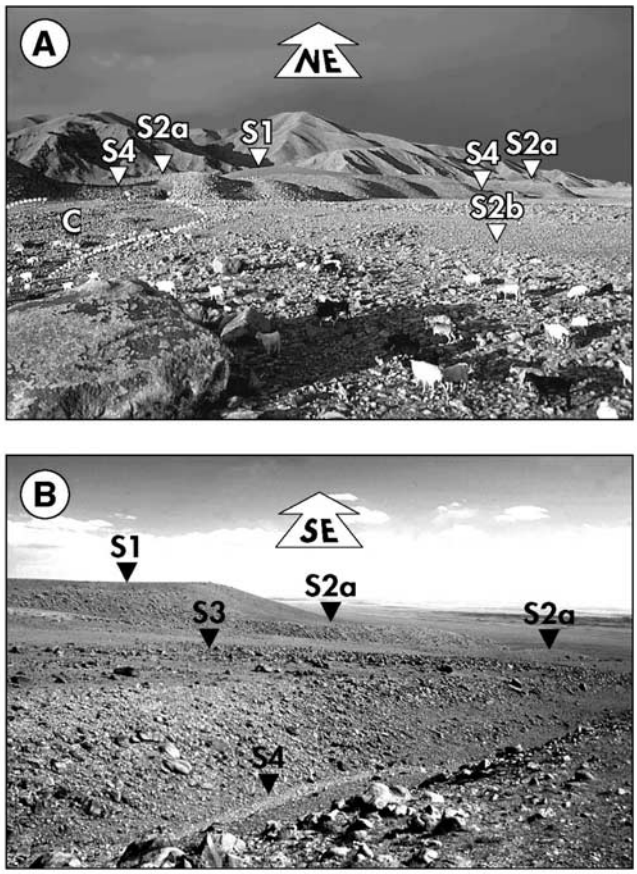

Figure 6. (a) View taken from downstream of the Gurvan Bulag fault scarp showing the system of inset surfaces. See orientation and location in Figure 5a. (b) The same area seen from a topographic ridges of surface S1 (2000 m altitude marker on Figure 5b).

possibility of accurately separating the offsets associated with two events. There is a slight indication of a bevel at the upper portion of this profile, suggesting a preexisting scarp. This feature also appears on the profile reported by *Kurushin et al.* [1997]. Therefore we interpret the very uppermost beveled part of profile 4 (between coordinates 100 and 150 m) as a remnant of preexisting topography.

[16] In summary, the mean 1957 vertical offset along the central part of the Gurvan Bulag thrust fault calculated from profiles 1, 2, and 3 is 4.2 ± 0.3 m. There is evidence for one preexisting earthquake affecting surface S4. The mean vertical offset of the penultimate event calculated from profiles 2 and 3 is 2.5 ± 1.2 m, which represents a lower limit because the scarps may have been affected by erosion or gravitational collapse. It is also likely that springs, present within S4 gullies along the fault scarp before 1957 (''Gurvan Bulag'' means ''three springs'' in Mongolian; the 1957 earthquake changed local hydrology and dried up the springs) and associated overland flow, as well as cryoturbation, have modified the shape of the scarp.

2.3.2. Offset of Surface S2

[17] Profiles 5 and 6 are parallel profiles 2 km long separated by about 10 m (Figures 4, 5, and 9), cross surface S2 and permit estimation of its cumulative vertical displacement. They show a planar surface at the footwall with a general slope of about 5° toward the south, then a cumulative vertical scarp corresponding to surface S2 which shows a slight convex upward bend just upslope the fault rupture. Within the foreberg, the debris flow surface S3 covers surface S2 and is characterized by a planar section that connects to the upstream slope of the fan.

[18] The downslope endpoints of profiles 5 and 6 are located far below the fault scarp to extend beyond localized

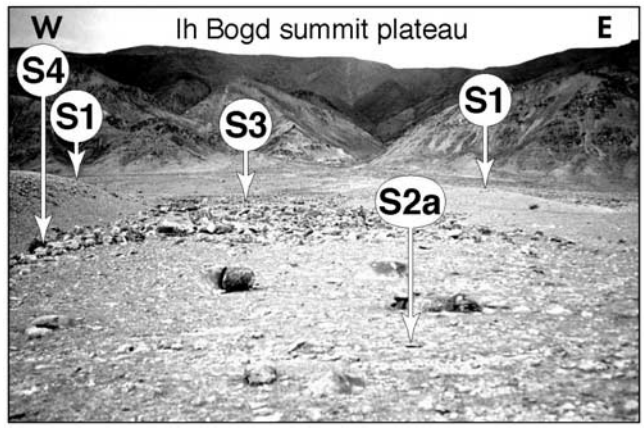

Figure 7. Surface S2 covered by the debris flow S3, which terminates upstream from the fault scarp.

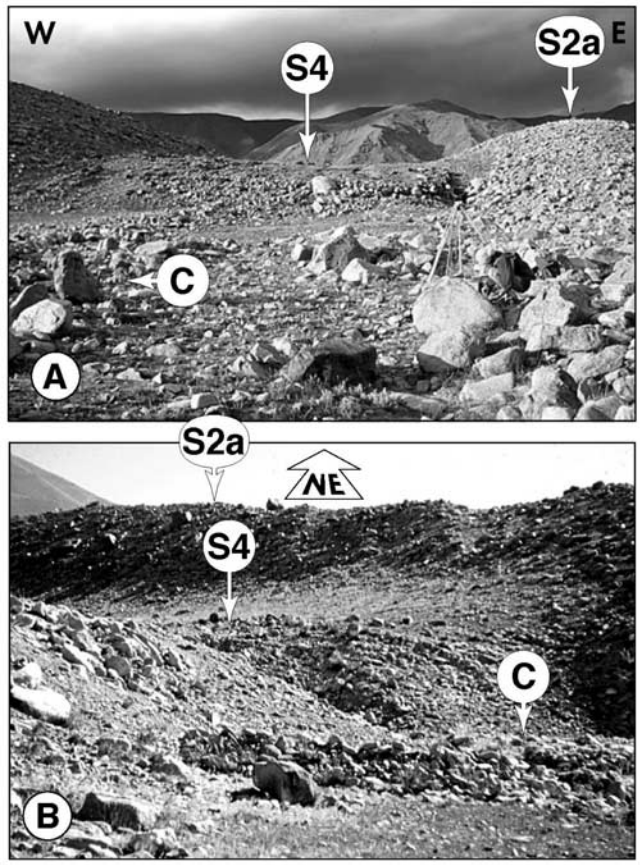

Figure 8. (a) Cut terrace surface S4 (profile 2, Figure 9b). (b) Cut terrace surface S4 (profile 4, Figure 9b).

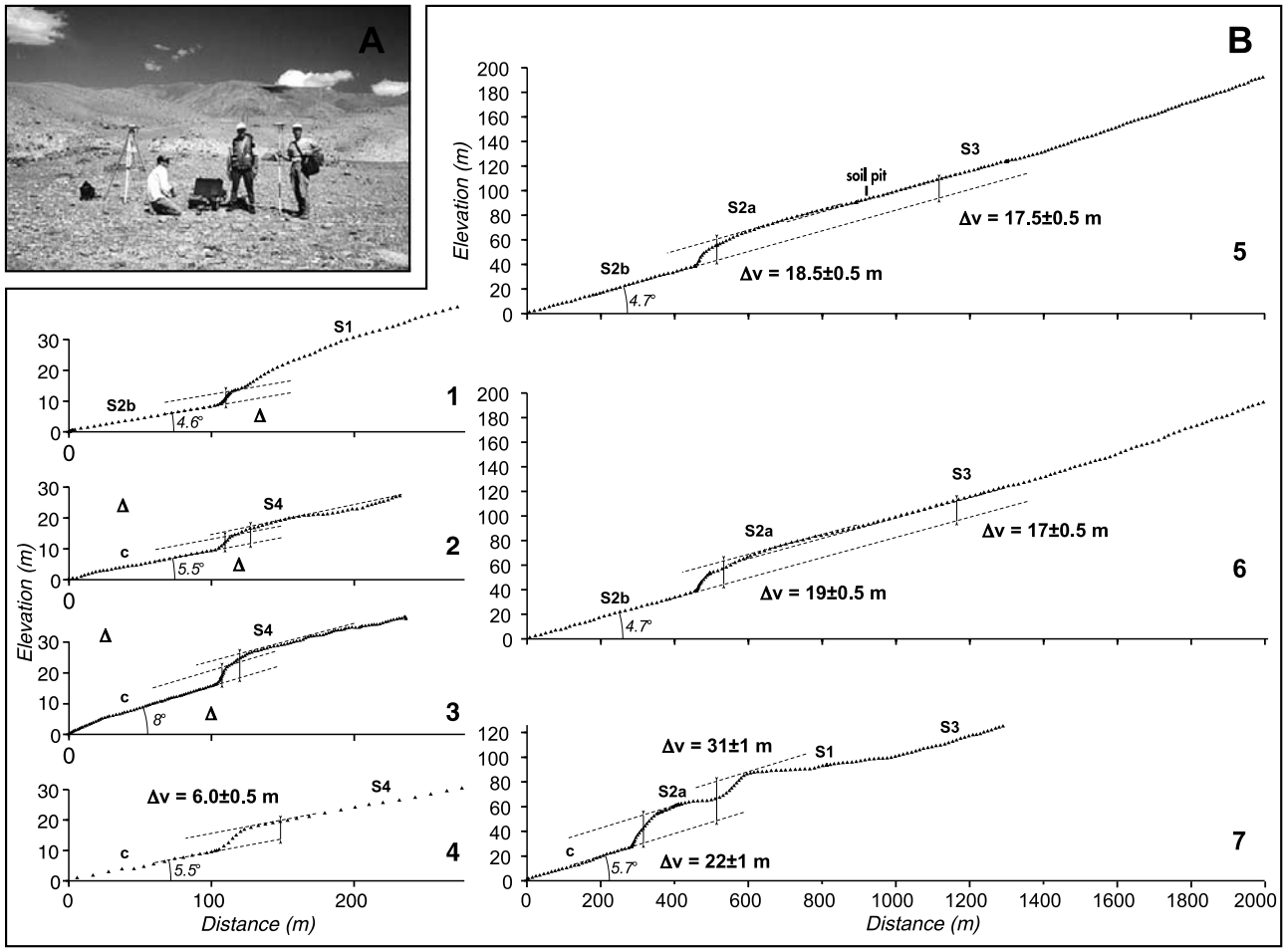

Figure 9. (a) Setting of GPS kinematics survey at the foothills of Gurvan Bulag thrust ridge. (b) Topographic profiles across uplifted surfaces.

cones (surface C) that overlie surface S2. Indeed, this site is within the surface defined as S2b from analysis of aerial photographs. Therefore we consider the vertical separation between the hanging wall surface S2a and the footwall surface S2b as the maximum cumulative vertical slip of surface S2. From profiles 5 and 6, we estimate this maximum cumulative vertical slip to be18.5 ± 0.5 and 19 ± 0.5 m, respectively.

[19] Profile 7 also crosses surface S2 and provides an estimate for a maximum vertical displacement of S2 of 22 ± 1 m. Further east, a similar cumulative vertical displacement for S2 (17–20 m) was measured along a profile that follows a well-preserved area of the surface on both sides of the rupture [*Carretier*, 2000]. In summary, from profiles 5, 6, and 7, we estimate the mean vertical offset for surface S2 in the studied area at 19.8 ± 1.9 m.

2.3.3. Offset of Surface S3

[20] Profiles 5 and 6 also permit estimation of the vertical displacement of surface S3, although this is more uncertain because at this place, S3 stops before reaching the fault scarp, and is not found at the footwall. In the hanging wall, S3 deposits are almost at the same level than surface of S2 deposits (see also Figure 7). The slight difference in height between the surfaces S2 and S3 on the profiles 5 and 6 may be interpreted as an inset of about 1 m of surface S3 with respect to the top of surface S2. It can also be interpreted as the termination of S3 deposits against the fold of surface S2 above the fault. Extension of the planar S3 surface to the south indicates vertical separations of 17.5 ± 0.5 and 17 ± 0.5 m of surface S3 deposits with respect to footwall surface S2b on profiles 5 and 6, respectively. As described earlier, S3 and S2 are deeply incised by gullies denoted S4 (Figures 5 and 6b), the formation of which led to a series of cones on the footwall (C). We interpret these features as the effects of regressive erosion caused by vertical displacement along the fault. However, because we do not observe the continuation of S3 all along the profile, we cannot tell how much of the observed cumulative displacement occurred before and after S3 deposition. Two extreme scenarios can be proposed depending on whether the cumulative offset occurred before or after S3 deposition. If most of the cumulative offset occurred before S3 deposits, the minimum vertical displacement for S3 would be 7.8 ± 0.4 m, which corresponds to the vertical displacement calculated for the closest S4 gully (profile 3, Figure 9b). In contrast, if the cumulative offset occurred after deposition, the measured mean vertical separation of 17.3 ± 0.4 m would represent a maximum value for the vertical offset for S3 (assuming that the footwall

Figure 10. Surface S2a and some sampling sites.

Figure 11. Granite boulders sampled from debris flow surface S3.

surface level of S3 would be the same as surface S2b). Finally, profile 7 gives a minimum vertical offset of S1 of 31 ± 1 m.

3. Estimating Surface Exposure Ages

3.1. Fieldwork and Sampling

[21] To date the exposure to cosmic rays of morphological markers, we had been measuring ^{10}Be produced in situ [e.g., *Brown et al.*, 1991; *Bierman*, 1994]. The alluvial fans cut by the Gurvan Bulag thrust fault show variations in morphology and degree of preservation (see description of studied sites previously). Our sampling selection strategy should minimize the effects of exposure prior to deposition and of erosion following deposition. We focused our work on the three most recent morphotectonic markers surface S2, the debris flow surface S3, and the cut terrace S4.

[22] S2 and S3 surfaces are depositional features characterized by boulder fields. We assumed that the occurrence of large granite boulder flows represent the effect of strong erosional events having reworked massive quantities of slope material from the upstream drainage basins of the Ih Bogd massif. In addition, because these debris flows represent an intense erosional event, it would be expected that deposition would be rapid and little cosmogenic nuclide accumulation would occur during transport. Under these conditions, the concentration of in situ cosmogenic ^{10}Be is directly related to the time when alluviation ended, or when subsequent incision led to the abandonment of the fan surface. All the samples are along profiles 5 and 6 (Figure 5b).

[23] We collected seven samples from surface S2, downhill of debris flow S3, where topographic surface forms a slight convex upward bend (see profiles 5 and 6 in Figure 9b), and where the boulders (∼1 m in diameter) are far apart: five samples were taken on top of granites boulders of this part of the surface and two samples from a soil pit showing Stage 3 carbonate morphology (Figures 5 and 10).

[24] We collected 10 samples from S3 debris flow surface sampling the top of granite boulders (∼1–3 m in diameter) (Figures 5 and 11). We also collected a depth profile of 10 samples from a 1.7 m deep soil pit located at the toe of debris flow S3 to analyze the distribution of ^{10}Be concentration at depth (Figure 12).

[25] Five cobbles were sampled from S4 cut terraces (Figures 5, 8a, and 13). We believe that this material corresponds to older fill material that was buried before its exposure by stream incision.

[26] In addition of the sampling of the three morphotectonic markers, we also collected five samples from the eastern wall of the riser which incised the debris flow S5

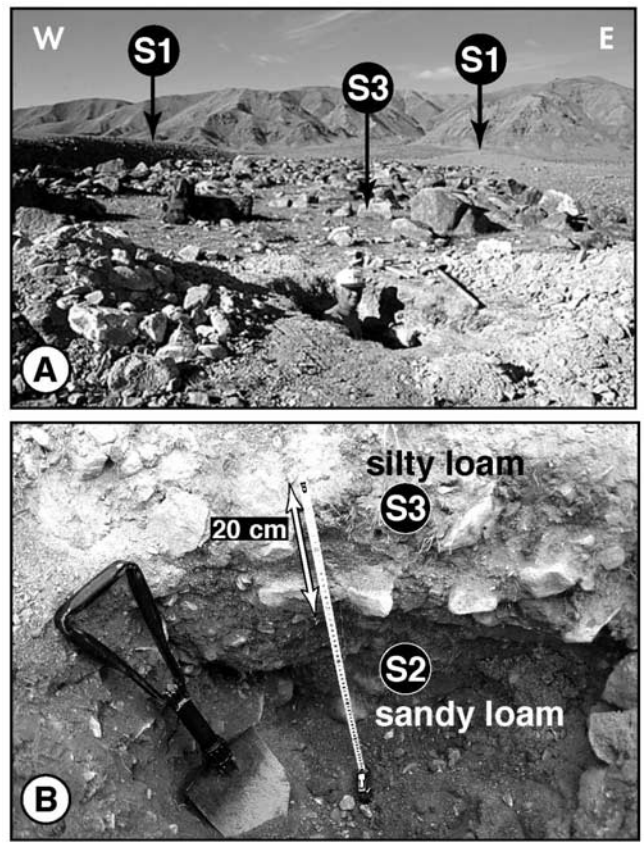

Figure 12. (a) View of the soil pit dug in surface S2 at the toe of debris flow surface S3. (b) Detailed photograph of the upper part of the soil pit showing the pedologic change corresponding to the contact between S3 and S2 materials.

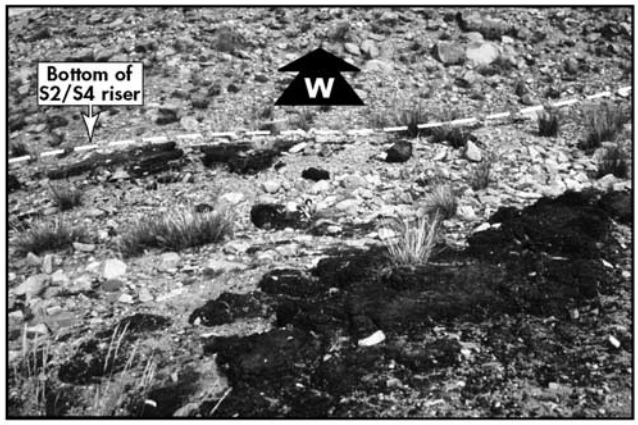

Figure 13. Photo showing some of the samples partly covered by dead moss within one of the S4 cut terraces.

(Figures 5 and 14). We used this natural cross section to analyze the ^{10}Be concentrations beneath 2 m depth.

3.2. Laboratory Methods

[27] Thirty-seven samples (Table 1) have been analyzed by accelerator mass spectrometry. Samples from surfaces S3, S4, and S5 as well as from the soil pit were analyzed at the Tandétron AMS facility, Gif-sur-Yvette, France [*Raisbeck et al.*, 1987, 1994]. Samples from surface S2 were analyzed at the LLNL AMS facility, Livermore, California, USA [*Davis et al.*, 1990].

[28] Chemical preparation varied slightly between the two laboratories. At Gif-sur-Yvette, it consisted of crushing and sieving samples to yield 0.25–1.0 mm fragments, which were cleaned in HCl to eliminate potential surface contamination by ^{10}Be produced in the atmosphere [*Brown et al.*, 1991]. Then quartz was purified from the cleaned material by selective dissolution of feldspars with H_2SiF_6. After quantitative dissolution of this purified quartz in HF, the samples were spiked with 300 μg of ^{9}Be carrier for analyses of ^{10}Be. Isotope ratios were determined by calibration against NIST Standard Reference Material 4325. At Livermore, samples were crushed and sieved to an uniform size of 0.25–0.5 mm. Quartz was separated from these

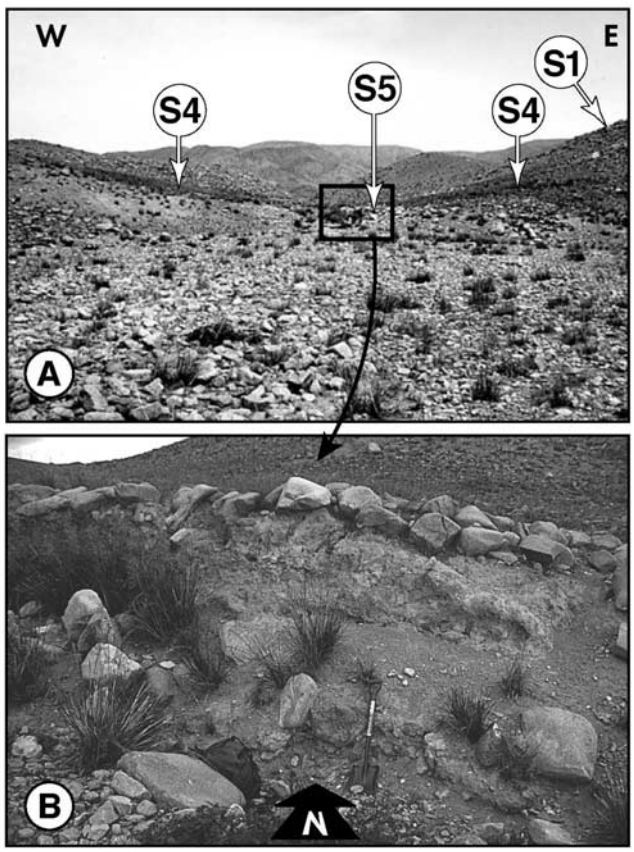

Figure 14. (a) View from downstream of a recent (post-1957) stream incision in a rock flow deposit S5, inset in a cut terrace S4. (b) The eastern riser of the incision into surface S5. Samples were taken at the base of the riser.

Table 1. ^{10}Be Concentrations and Ages for Markers

Sample ID	^{10}Be × 10^3, atm/g[a]	Uncertainty, 1σ
S2 samples (altitude: 2000 m, latitude: 44°50.832′N, production: 27.4 atm/g/yr)		
GB96-9	3480	118
GB96-10	3640	115
GB96-11	3630	89
GB96-12	3410	83
GB96-13 (65cm)	1360	39
GB96-14 (90cm)	960	32
GB96-13 (0cm)[b]	3360	349
GB96-14 (0cm)[b]	3410	360
GB96-15[c]	2400	58
Mean concentration	3488	120
Mean ^{10}Be age, ka	131	20
S3 samples (altitude: 2000 m, latitude: 44°50.832'N, production: 27.4 atm/g/yr)		
Mo93-AII1	325	36
Mo93-AII2	336	49
Mo93-AII3	488	52
Mo93-AII4	677	65
Mo93-AII5[c]	1166	99
Mo95-11	426	37
Mo95-12	335	27
Mo95-13	368	29
Mo95-14	482	61
Mo95-15	505	37
Mean concentration	438	114
Mean ^{10}Be age, ka	16.0	4.8
S4 samples (altitude:1950 m, latitude: 44°50.832'N, production: 26.5 atm/g/yr)		
Mo95-16	121	13
Mo95-17	235	31
Mo95-18	91	15
Mo95-19	146	20
Mo95-20[c]	414	36
Mean concentration	148	62
Mean ^{10}Be age, ka	5.6	2.5
S5 samples		
Mo95-21	1589	102
Mo95-22	490	43
Mo95-23	350	34
Mo95-24	467	45
Mo95-25	405	45

[a]All results presented with respect to ICN standards. For S3, S4, and S5 samples, this requires normalization by a factor of 1.14 ± 0.04 to account for inconsistency with NIST standards.

[b]Normalized to surface with a neutron attenuation length of 145 ± 7 g/cm^2 and a density of 2.0 ± 0.1 g/cm^3.

[c]Not included in calculation of mean.

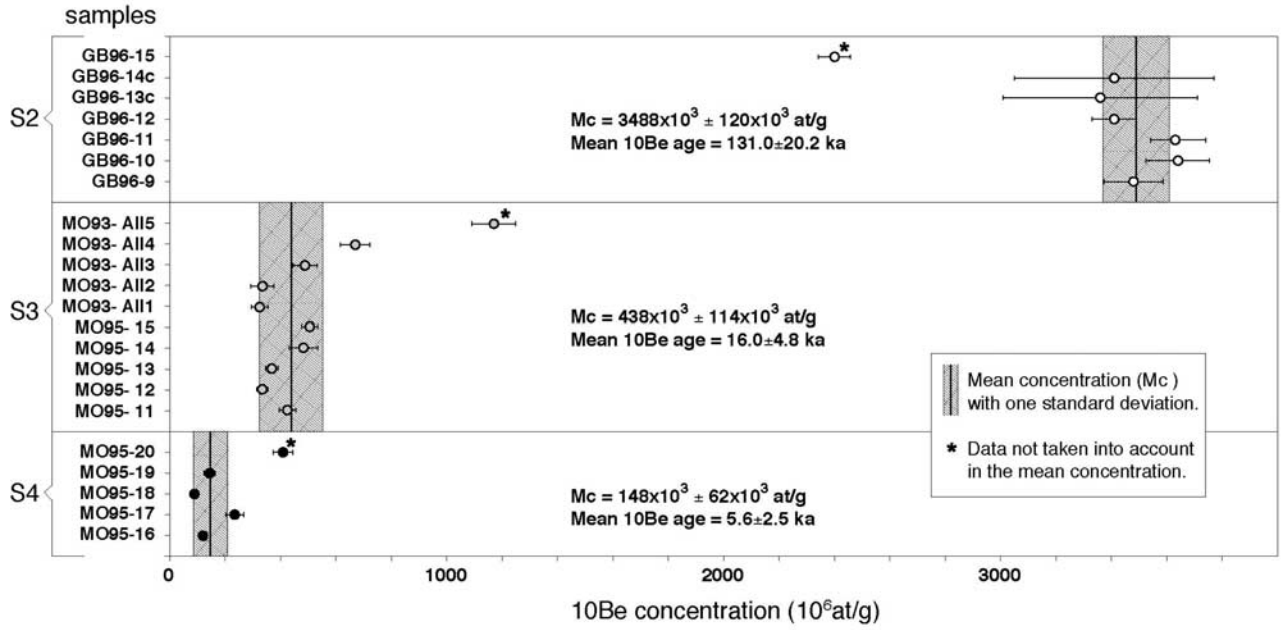

Figure 15. Diagram showing ^{10}Be concentrations exposure ages for the three sampled surfaces.

rocks by a chemical isolation method [*Kohl and Nishiizumi*, 1992] using HCl and HF:HNO_3 baths. Beryllium carrier was added to the clean quartz separates and the sample was then dissolved in an HF:HNO_3 mixture. Be was separated and purified using ion exchange chromatography. The observed ratios were normalized to ICN ^{10}Be standards that were diluted by Nishiizumi (personal communication, 1992). It appears that comparison of ^{10}Be concentrations determined using ICN standards are slightly higher than those determined by calibration against the NIST standard and require normalization by a factor of 0.875 ± 0.030 [e.g., *Middleton et al.*, 1993]. Interlaboratory calibration of ^{10}Be determinations should resolve these inconsistencies. We present all measurements calibrated relative to the ICN standards, as these have been utilized for determination of ^{10}Be production rates (Table 1). Our calculations are based on the assumption that there has been little erosion from the sampled boulder surfaces; this is supported by the presence of heavy desert varnish coatings. Nevertheless, this assumption makes our ages lower limits.

[29] For each of the three surfaces, we observe clusters of data that do not overlap from one surface to another (Figure 15). However, two samples, M093-AII5 and M095-20, show much higher concentrations than the rest of S3 and S4 samples, respectively. We interpreted these samples as reworked material from preexposure [e.g., *Van der Woerd et al.*, 1998; *Brown et al.*, 2002]. It is likely, for instance, that sample M095-20 from surface S4 is reworked material from the S3 debris flow. On the other hand, GB96-15 has low ^{10}Be concentrations compared with other S2 samples. This sample was taken at the top of a weathered boulder almost totally encased in the ground surface, (Figure 10, foreground). We interpret this lower concentration as the result of shielding by debris covering the boulder and gradually removed over time [cf. *Hallet and Putkonen*, 1994]. The three samples (of the 22 analyzed for surfaces S2, S3, and S4) that fall outside the cluster values were not taken into account in discussions that follow.

3.3. Age Calculations

3.3.1. Alluvial Surfaces

[30] From the mean concentration of the clustered values, we calculated ages and associated uncertainties propagating an uncertainty of 15% in the production rate. The production rate of ^{10}Be was estimated from the altitude- and latitude-dependant polynomials of *Lal* [1991]. The mean concentrations calculated for surfaces S2 (six samples), S3 (nine samples), and S4 (four samples) are 3488 ± 120 × 10^3, 438 ± 114 × 10^3, and 148 ± 62 × 103 atm/g, respectively (Figure 15). From these concentrations, the ages for the end of deposition or abandonment of S2 and S3 are 131 ± 20 and 16.0 ± 4.8 ka, respectively, and the exposure age of S4 is 5.6 ± 2.5 ka.

3.3.2. Soil Profile

[31] Distributions of ^{10}Be concentrations in the 1.7 m soil pit excavated at the toe of debris flow S3 shows a log linear decrease in ^{10}Be concentrations with depth (Figure 16 and Table 2). This material thus belongs to the same depositional sequence and underwent the same evolution in situ since the time of deposition. The concentrations are much higher than would be expected for a profile within surface S3, indicating another origin. On the other hand, the distribution is nearly consistent with the mean concentration estimated for surface S2. The slightly higher concentrations of S2 surficial material with respect to the log linear depth profile (Figure 16) suggests that ~25 cm of S2 deposits may have been eroded during the emplacement of the S3 debris flow. This is consistent with the pedogenic profile along the soil pit showing a change in texture at depth, from silty loam to underlying sandy loam, that can be attributed to a depositional unconformity. This overlying deposition could be the fine-grained portion of the debris flow associated

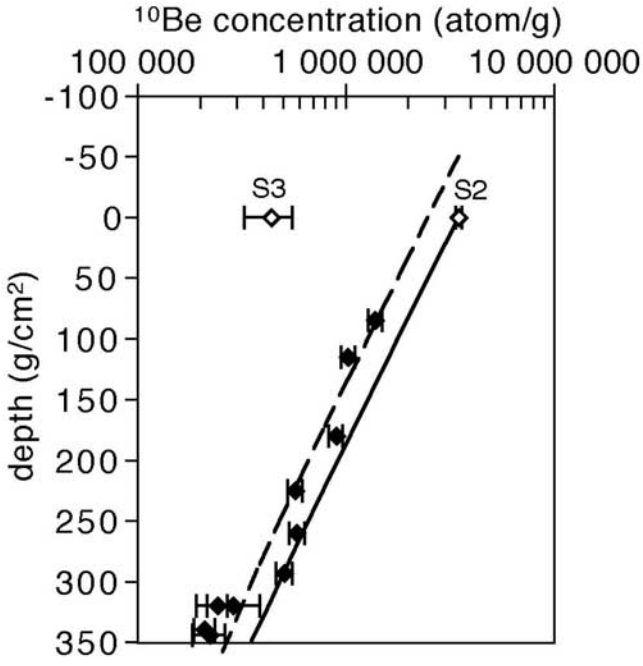

Figure 16. ^{10}Be concentration as a function of depth in the soil pit (closed symbols) and mean concentrations for surfaces S2 and S3 (open symbols). A theoretical curve is presented for depth evolution of S2 material (solid line). The exponential decrease with depth of ^{10}Be in soil pit samples indicates that these samples have had the same relative positions during most of their exposure history and were deposited during a short period of aggradation. The mean concentration of S3 surface samples is far lower than those of the underlying samples, indicating that S3 material was deposited atop a much older surface. The coherence between S2 surface materials and the soil profile suggest that it was the older surface upon which S3 was deposited. However, the concentrations in surface S2 are slightly higher than would be expected from the depth profiles, suggesting the possibility of a net removal of 50 g/cm^2 (~25 cm) at the time of deposition of surface S3 (dotted line).

with surface S3. Its thickness at this place is about 20 cm (Figure 12b). This abrupt change of texture was also observed at the same depth in a soil pit excavated 20 m farther north in the S3 boulder field. All this support the hypothesis that S2 samples contained negligible inherited ^{10}Be upon deposition and that its surface exposure age is correct. Therefore our interpretation is that surface S2 deposition ended at ~131 ka and remained exposed to cosmic rays during the late Pleistocene (~115 kyr) before it was covered by abrupt emplacement of S3 debris at ~16 ka.

3.3.3. Recent Debris Flow

[32] Samples collected at the bottom (≥2 m depth) of the recent debris flow associated with S5 show unexpectedly high ^{10}Be concentrations ranging from 350 ± 45 × 10^3 to 1589 ± 102 × 10^3 atm/g (Table 1). If we assume that the material was not exposed prior to deposition, such values at depth would suggest that the deposits remained exposed to cosmic rays at the present position for hundreds of thousands of years. The inset position of the debris flow in other surfaces precludes this scenario and implies, on the contrary, that most of the material was previously exposed. Careful analysis of the drainage pattern associated with S5 shows that the debris flow deposits are confined to the mainstream channel draining the fan (Figure 4). No equivalent recent debris flow was observed inset into other nearby S4 surfaces that drain only the lower reaches of the fan surface (Figure 5b). Therefore we interpret S5 material as a localized deposition associated with remobilization processes within the main drainage. Note that four of the five samples have concentrations similar to S3 concentrations which suggests that most of S5 material is a recent reworking of upstream S3 material confirming that a major alluviation occurred at ~16 ka.

4. Slip Rates in the Late Pleistocene and the Holocene

[33] Topographic data and ^{10}Be dates of offset surfaces allow us to calculate vertical slip rates along this part of the Gurvan Bulag thrust fault (Figure 17). Abandonment or the end of deposition of surface S2 in the studied place is dated at 131 ± 20 ka and its mean vertical offset is estimated at 19.8 ± 1.9 m. Of this total offset, 20–25% is due to the 1957 event (4.2 ± 0.3 m). Because one cannot know when during the seismic cycle the marker formed, we bracketed the late Pleistocene-Holocene slip rates with mean total offset (19.8 m) and mean total offset minus the mean 1957 offset (15.6 m). Dividing these values by the age of S2 yields upper and lower limits on the vertical slip rates of 0.16 ± 0.04 and 0.12 ± 0.03 mm/yr, respectively. We adopt a value of 0.14 ± 0.03 mm/yr for the vertical component of the slip.

[34] The end of deposition of surface S3 is dated at 16 ± 4.8 ka. Depending on whether most of the offset occurred before or after S3 deposition (see section 2.3.3), the vertical offset is estimated to be 7.8 ± 0.4 or 17.3 ± 0.4 m. These values incorporate the 1957 offset. As noted previously, we do not know when the marker formed in the seismic cycle. Following the same line of reasoning as for surface S2, we bracket the vertical offset of S3 between 7.8 and 3.4 m or 17.4 and 13.1 m. Dividing these values by the age of S3 deposits, we obtained two vertical slip rates for the last ~16 kyr, 0.40 ± 0.11 and 1.05 ± 0.25 mm/yr, respectively.

[35] Whichever hypothesis we choose, whether most of the displacement observed on profiles 5 and 6 occurred before or after S3 deposits, it appears that the vertical slip

Table 2. Depth Profile in Surfaces S3 and S2

Sample ID	^{10}Be × 10^3, atm/g[a]	Uncertainty, 1σ
GB96-1 (40–45 cm)	1383	109
GB96-2 (55–60 cm)	1022	78
GB96-3 (90 cm)	895	69
GB96-4 (110–115 cm)	570	45
GB96-5 (130 cm)	582	51
GB96-6 (145–148 cm)	504	46
GB96-7A (160 cm)	288	98
GB96-7B (160 cm)	241	27
GB96-8A (170 cm)	209	24
GB96-8B (172 cm)	222	40

[a]All results presented with respect to ICN standards. This requires normalization by a factor of 1.14 ± 0.04 to account for inconsistency with NIST standards.

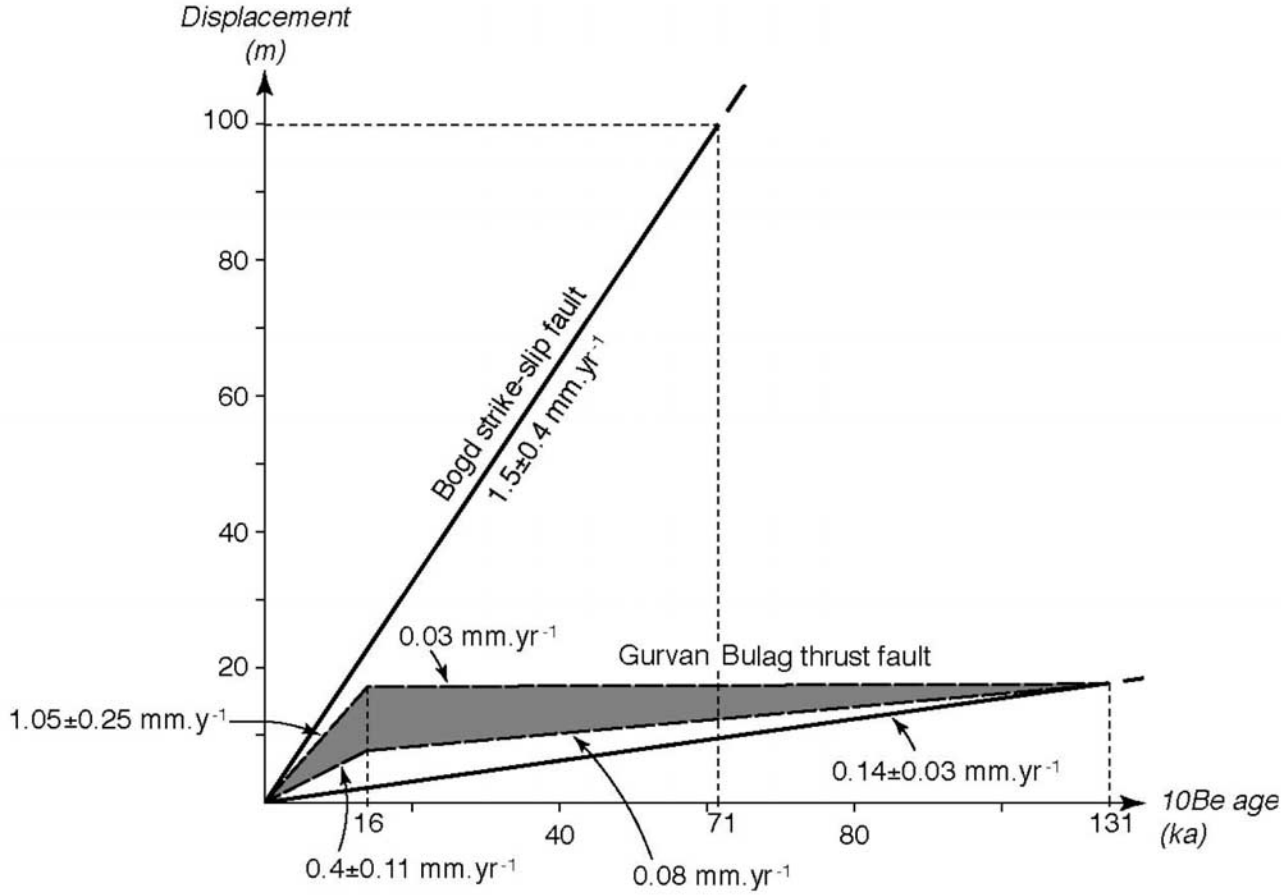

Figure 17. Rates of horizontal and vertical slip along the Bogd strike-slip fault and the Gurvan Bulag thrust fault, respectively, during the late Quaternary.

rate of the Gurvan Bulag fault increases at the end of late Pleistocene (Figure 17). If we choose the first interpretation, and subtract 7.8 from 19.8 m, the late Pleistocene, between 131 and 16 ka, vertical slip rate is ~0.08 mm/yr, which is five times smaller than for the last ~16 kyr (~0.4 mm/yr). The recurrence intervals for events similar to 1957 earthquake would be about 50 kyr during the late Pleistocene and 10.4 ± 3.6 kyr during the last ~16 kyr.

[36] If we choose the second interpretation, and if we subtract 17.3 m (S3 offset) from 19.8 m (S2 offset), the late Pleistocene vertical slip rate is ~0.03 mm/a. Consequently, the Gurvan Bulag slip rate would have increased drastically at the end of the late Pleistocene. This has important significance in terms of seismic activity. If we assume repeated surface ruptures similar to that of 1957 (4.2 m), the Gurvan Bulag thrust fault would have remained mainly quiescent during the late Pleistocene period, with maximum one strong event. In contrast, there would have been four events during the last ~16 kyr, with a recurrence interval of 4 ± 1.2 kyr.

[37] Surfaces S4 are vertically displaced with 6.5 ± 1.2 m with respect to the footwall surfaces. From topographic profiles, we interpreted this displacement as the cumulative slip due to only two events, the penultimate and the 1957 surface ruptures, and thus has limited use for a rate determination. However, the exposure age of S4 cobbles (5.6 ± 2.5 ka) may represent the age of the erosional surface that was established between the prepenultimate and penultimate events. This furnishes an upper limit for the time interval between the penultimate event and 1957 earthquake.

5. Discussion and Conclusion

5.1. Regional Climate History

[38] Our ^{10}Be dates indicate that two most recent major aggradational episodes on the southern slopes of the Ih Bogd massif occurring at 131 ± 20 and 16 ± 4.8 ka (Figures 18a and 18c), may be contemporaneous with global climatic changes at the terminations of marine isotope stages (MIS) 6 and 2, respectively. Consistent with earlier work in the Gobi-Altay [*Ritz et al.*, 1995; *Carretier*, 2000], the ca. 100 ka event appears to have been of greater magnitude than subsequent events. The beginning of the late Quaternary (MIS 5e) was characterized by exceptional global warmth and coincides with a period of strong Milankovitch global warming centered on 125,000 BP and lasting between 134,000 and 120,000 BP [*Dawson*, 1992]. Similarly, a period of global warming which began near 15,000 BP during the MIS 2/1 transition also corresponds to an enhanced period of insolation. In the Gobi-Altay, cold periods may have been too dry to permit significant glaciation [e.g., *Gillespie and Molnar*, 1995] and the temperature too low to allow major alluviation processes. This is

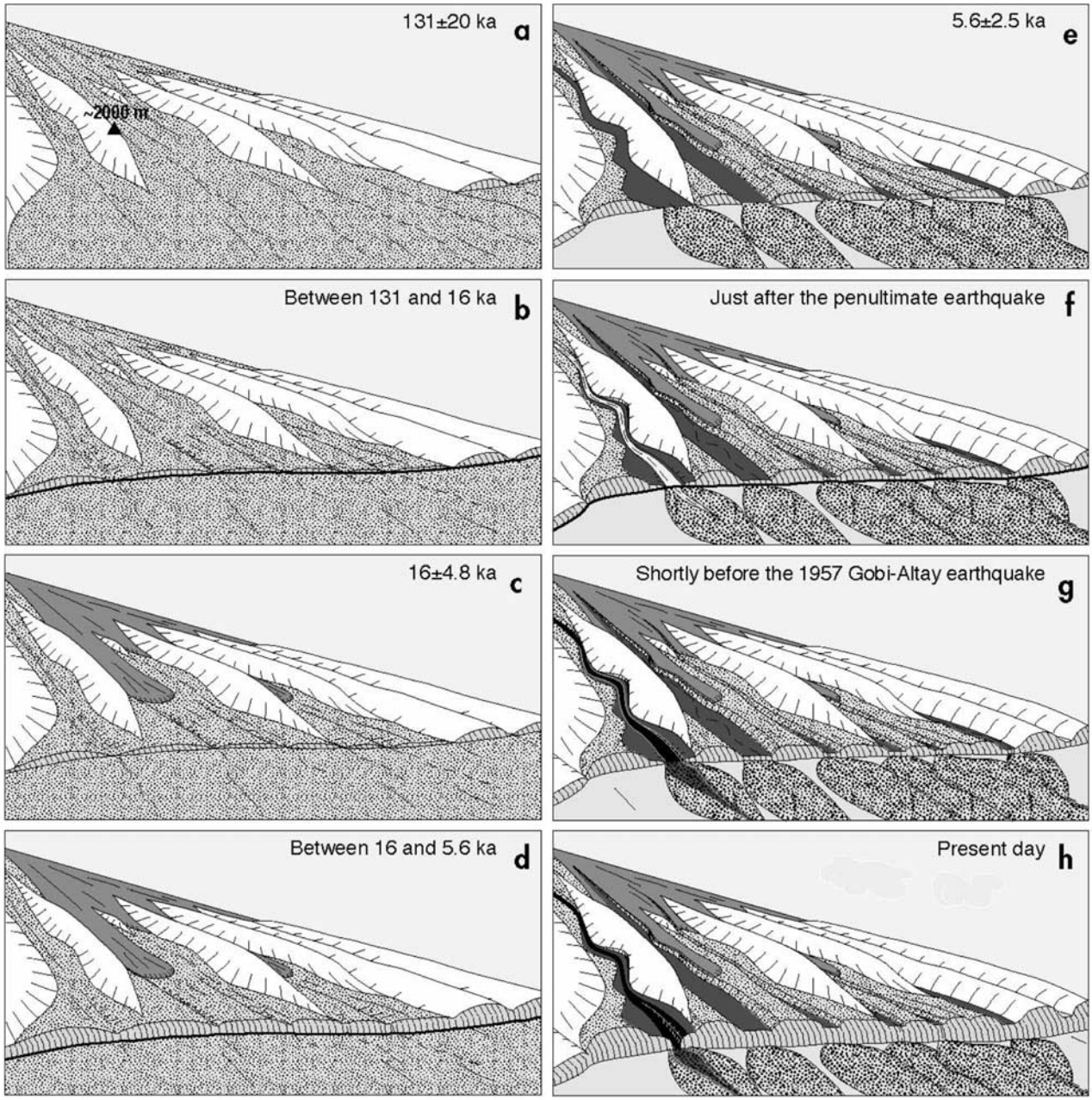

Figure 18. Scenario of interactions among alluvial deposition, vertical slip, and stream incision within the Gurvan Bulag thrust fault study site. (a) Deposition of surface S2 inset into older topography S1. (b) Exposure of surface S2 during a period with very low fault activity and no aggradation. (c) Deposition of debris-flow surface S3 (the slight bend of S2 above the fault halts the flow). (d) Period of increasing fault activity. (e) Formation of cut terraces S4 and corresponding localized depositional cones C downstream the fault scarp. (f) Incision of cut terraces S4 within the mainstream channel subsequent to the penultimate earthquake. (g) Deposition of a minor rock-flow S5 within the mainstream channel. (h) The 1957 event followed by rapid incision of the rock-flow S5 within the mainstream channel.

consistent with preliminary dates of fine deposits (S. Balescu, personal Communication, 2002) that accumulated behind the gigantic Baga Bogd paleolandslide [*Philip and Ritz*, 1999] that suggest that no important alluviation events occurred between ca. 90 and 16 ka at the foothills of the Baga Bogd massif.

[39] Consistent with previous field surveys [i.e., *Florensov and Solonenko*, 1965], we did not observe any glacial features (such as cirques, rock bars, or moraines) during a total of 14 weeks of fieldwork in the Ih Bogd and Baga Bogd mountains over six field seasons. This suggests that the major aggradation events at the terminations of MIS 6 and MIS 2 were not associated with glacial meltwater, but rather that there was enhanced precipitation in the Gobi-Altay at these times. The interpretation of a major climatic pulse at 16 ± 4.8 ka is consistent with conclusions by *Owen et al.* [1997,

1998] concerning the end of permafrost and return of stream incisions in the region at 13–10 ka.

[40] These results are in good agreement with those found north of Ih Bogd massif East of the Dalan Türüü foreberg (Figure 2), where a morphotectonic feature similar to the S2 surface at Gurvan Bulag was dated using ^{10}Be produced in situ at ~100 ka [*Hanks et al.*, 1997]. These pulses of aggradation are also evidenced along the Bogd strike-slip fault at Noyan Uul (Figure 2), where the interaction between the horizontal displacement along the fault and the fan sequences shows that aggradation events are separated by long nondepositional periods [*Ritz et al.*, 1995; *Carretier et al.*, 1998].

5.2. Neotectonics of the Gurvan Bulag Fault

5.2.1. Variation of Slip Rates During the Late Pleistocene-Holocene

[41] Our results suggest evolution of the vertical slip rate along the Gurvan Bulag thrust fault over the last ~131 kyr (Figure 17). They indicate an increase of the fault activity at the end of the late Pleistocene, which is more or less pronounced, depending upon the offset chosen for surface S3. However, whether this increase is modest with a fault evolving from low activity (0.08 mm/yr) to moderate activity (0.4 mm/yr), or large with a fault evolving from quasi-inactivity (0.03 mm/yr) to high activity (1.05 mm/yr) [e.g., *Slemmons and Depolo*, 1986] cannot be deciphered from our morphologic observations.

[42] Recurrence intervals may be used to evaluate which of these scenarios is more appropriate. The value of 5.6 ± 2.5 kyr for the maximum time interval between the penultimate event and 1957 earthquake estimated from analyses of surface S4 is consistent with the recurrence interval (4.0 ± 1.2 kyr) for events similar to that of 1957 implied by the high slip rate calculated for the last ~16 kyr. Furthermore, *Prentice et al.* [2002] show that the penultimate event occurred after 6.0 ka, most likely between 2.6 and 4.4 ka, and that a possible earlier rupture occurred after 7.3 ka. This implies that 1.05 ± 0.25 mm/yr may be the better estimate for the Holocene rate of vertical slip along the Gurvan Bulag thrust fault.

5.2.2. Comparison of Activity on the Bounding Faults of the Ih Bogd Massif

[43] These results also suggest that the recurrence intervals for the last ~16 kyr surface faulting on the Gurvan Bulag thrust are similar to the Bogd strike-slip fault. Indeed, at Noyan Uul, *Ritz et al.* [1995] estimated a minimum slip rate at 1.2 mm/yr from an ~100 m offset alluvial dated at 80 ka. A reevaluation of the production of ^{10}Be calculated for the geographic, rather than geomagnetic latitude of the site (the average location of the geomagnetic North Pole over the past 10 ka is very close to the geographic North Pole [*Ohno and Hamano*, 1992]) yields a minimum age of 71 ± 12 ka for the alluvial surface and consequently, a 1.5 ± 0.4 mm/yr long-term maximum horizontal slip rate along the Bogd fault. This includes a 10 m uncertainty in the horizontal measurement and a 15% uncertainty on the production rate. At Noyan Uul, differential GPS surveys of mismatched gullies indicate a horizontal offset of 5.5 ± 0.5 m for the1957 event and a double displacement of 11 ± 1 m for the combined 1957 and penultimate events [*Ritz et al.*, 1997]. A 5.5 m characteristic horizontal offset [cf. *Schwartz and Coppersmith*, 1984] along the Bogd fault, implies a minimum recurrence interval of 3.7 ± 1.3 ka, similar to our value for Gurvan Bulag. In contrast with the possible relationship noted here, *Prentice et al.* [2002] conclude that the penultimate surface ruptures of the Gurvan Bulag thrust and the Bogd faults did not occur during the same earthquake, based on paleoseismic data for the segment of the Bogd fault near Toromhon (Figure 2) indicating that the penultimate event occurred at 0.8–2.3 ka [*Bayasgalan*, 1999].

[44] Our late Pleistocene-Holocene vertical slip rate along the Gurvan Bulag fault is very close to a value reported for the northern flank of Ih Bogd. Using ^{10}Be and ^{26}Al produced in situ, *Hanks et al.* [1997] reported a ~0.1 mm/yr vertical slip rate for the past 100 ka along a thrust fault segment to the north of the massif, southeast of Dalan Türüü foreberg (Figure 2). This is consistent with the horizontal geometry of the summit plateau of Ih Bogd, which is interpreted as an uplifted, old, erosional surface (Figure 3) with identical cumulative slip on both sides.

[45] Could this imply that the activity of the thrust fault bounding the northern flank of the Ih Bogd massif had the same increase at the end of the late Pleistocene as the Gurvan Bulag thrust fault? The surface rupture of the 1957 earthquake produced vertical offset of about 2–3 m [*Kurushin et al.*, 1997] along the segment of the Bogd fault bounding the Ih Bogd massif to the North. If we assume a mean recurrence interval of ~3.5 kyr deduced from the late Pleistocene-Holocene slip rate along the Bogd fault (see earlier), this would lead to a vertical slip rate close to 1 mm/yr. This is similar to the last ~16 kyr slip rate at Gurvan Bulag and could mean that the fault segment bounding the Ih Bogd massif to the north also increases its activity at the end of the late Pleistocene.

[46] The ~0.14 mm/yr late Pleistocene-Holocene vertical slip rate along the thrust faults bounding Ih Bogd compared with the ~1.5 mm/yr late Pleistocene-Holocene horizontal slip rate along the main strike-slip segment of the Bogd fault poses the question of the distribution of the fault activity around Ih Bogd massif through time. One might imagine that the Bogd strike-slip fault moved alone for a long period of time, whereas no movement occurred along adjacent thrust fault segments. Alternatively, it is possible that the lateral movement occurring along the Bogd fault could be absorbed on other thrusts to achieve a 1 mm/yr long-term vertical slip rate of the Ih Bogd massif. Although satellite imagery and field observations suggest that the massifs associated with the Bogd fault contain several abandoned faults corresponding to thrust-related structures that accommodated regional oblique-slip deformation during earlier stages of tectonic activity [*Bayasgalan et al.*, 1999b], we do not know when these structures were active and what were their slip rates.

[47] However, if we assume that the late Pleistocene-Holocene vertical slip rate calculated along the Gurvan Bulag thrust fault represents the uplift rate for the Ih Bogd massif from the beginning of the deformation, the ~2 km of vertical separation between the summit plateau and the bounding faults would have occurred over a period of 12–18 Myr. This would imply extremely low erosion rate in this part of Mongolia. Moreover, it is an order of magnitude greater than had been assumed earlier by *Florensov and*

Solonenko [1965] and *Baljinnyam et al.* [1993], and is double the estimate of *Kurushin et al.* [1997]. Alternatively, if the slip rate during the last ~16 kyr were representative of the long-term, the time required for uplift of the Ih Bogd massif would be ca. 2 Myr. This emphasizes the need for knowledge of tectonic processes over a range of timescales for understanding mountain building.

[48] **Acknowledgments.** We thank B. Bayasgalan, K. Berryman, R. Braucher, K. Hanson, J. Jackson, W. Lund, C. Prentice, and T. Rockwell for fruitful discussions during field work, P. Molnar for his comments, and A. Delplanque for drawings. We thank Hubert Camus for helpful discussions about the geomorphology of alluvial deposits, and J. Van der Woerd and an anonymous reviewer for their thorough reviews that allowed us to make significant improvements to the original manuscript. This work was mainly supported by CNRS programs Tectoscope, Mecalith, DBT II, and Prose, by Lawrence Livermore National Laboratory (LLNL) operating under US DOE contract EN6-7405 and by USGS Menlo Park the Center of Informatic and Remote Sensing, Mongolian Academy of Sciences. Tandétron operation is supported by CNRS, IN2P3, and CEA.

References

Baljinnyam, I., et al., Ruptures of major earthquakes and active deformation in Mongolia and its surroundings, *Geol. Soc. Am. Mem.*, *181*, 62 pp., 1993.

Bayasgalan, A., Active tectonics of Mongolia, Ph.D. thesis, 182 pp., Univ. of Cambridge, Cambridge, 1999.

Bayasgalan, A., J. Jackson, J.-F. Ritz, and S. Carretier, Field examples of strike-slip fault terminations in Mongolia and their tectonic significance, *Tectonics*, *18*, 394–411, 1999a.

Bayasgalan, A., J. Jackson, J.-F. Ritz, and S. Carretier, 'Forebergs', flowers structures, and the development of large intra-continental strike-slip fault: The Gurvan Bogd fault system in Mongolia, *J. Struct. Geol.*, *21*, 1285–1302, 1999b.

Bierman, P. R., Using in situ produced cosmogenic isotopes to estimate rates of landscape evolution: A review from the geomorphic perspective, *J. Geophys. Res.*, *99*, 13,885–13,896, 1994.

Brown, E. T., J. M. Edmond, G. M. Raisbeck, F. Yiou, M. D. Kurz, and E. J. Brook, Examination of surface exposure ages of Antarctic moraines using in-situ produced ^{10}Be and ^{26}Al, *Geochim. Cosmochim. Acta*, *55*, 2269–2283, 1991.

Brown, E. T., R. Bendick, D. L. Bourlès, V. Gaur, P. Molnar, G. M. Raisbeck, and F. Yiou, Slip rates of the Karakorum fault, Ladakh, India, determined using cosmic ray exposure dating of debris flows and moraines, *J. Geophys. Res.*, *107*(B9), 2192, doi:10.1029/2000JB000100, 2002.

Bucknam, R. C., and R. E. Anderson, Estimation of fault-scarp ages from a scarp-height-slope-angle relationship, *Geology*, *7*, 11–14, 1979.

Carretier, S., Cycle sismique et surrection de la chaîne de Gurvan Bogd (Mongolie): Approche de la geomorphologie quantitative, Ph.D. thesis, 324 pp., Univ. of Montpellier II, Montpellier, 2000.

Carretier, S., F. Lucazeau, and J.-F. Ritz, Approche numérique des intéractions entre climat, faille active et érosion, *C. R. Acad. Sci. Paris*, *326*, 391–397, 1998.

Carretier, S., J.-F. Ritz, J. Jackson, and A. Baysagalan, Morphological dating of cumulative reverse fault scarp, examples from the Gurvan bulag fault system, Mongolia, *Geophys. J. Int.*, *148*, 256–277, 2002.

Cunningham, D. W., B. F. Windley, D. Dorjnamjaa, G. Badamgarov, and M. Saandar, A structural transect across the Mongolian Western Altai: Active transpressional mountain building in central Asia, *Tectonics*, *15*, 142–156, 1996.

Cunningham, D. W., B. F. Windley, L. A. Owen, T. Barry, D. Dorjnamjaa, and J. Badamgarav, Geometry and style of partitioned deformation within a late Cenozoic transpressional zone in the eastern Gobi Altai Mountains, Mongolia, *Tectonophysics*, *277*, 285–306, 1997.

Davis, J. C., et al., Lawrence Livermore National Laboratory—University of California Center for Accelerator Mass Spectrometry facility and research program, *Nucl. Instrum. Methods*, *B52*, 269–272, 1990.

Dawson, A. G., *Ice Age Earth: Late Quaternary Geology and Climate*, p. 293, Routledge, New York, 1992.

Florensov, N. A., and V. P. Solonenko, *The Gobi-Altai Earthquake* (in Russian) Moscow, Akademiya Nauk USSR, p. 391, 1963. (English translation, p. 424, Isr. Program for Sci. Transl., Jerusalem, 1965.)

Gillespie, A., and P. Molnar, Asynchronous maximum advances of mountain and continental glaciers, *Rev. Geophys.*, *33*, 311–364, 1995.

Grant, L. B., and K. Sieh, Paleoseismic evidence of clustered earthquakes on the San Andreas fault in the Carrizo Plain, California, *J. Geophys. Res.*, *99*, 6819–6841, 1994.

Hallet, B., and J. Putkonen, Surface dating of dynamic landforms; young boulders on aging moraines, *Science*, *265*, 937–940, 1994.

Hanks, T., J.-F. Ritz, K. Kendrick, R. C. Finkel, and C. D. Garvin, Uplift rates in a continental interior: Faulting offsets of a ~100 Ka abandoned fan along the Bogd fault, southern Mongolia, Proc. of Pensose Conf. on Tecton. Cont. Inter., Sept. 1997.

Hanks, T. C., R. C. Bucknam, K. R. Lajoie, and R. E. Wallace, Modification of wave-cut and faulting-controlled landforms, *J. Geophys. Res.*, *89*, 5771–5790, 1984.

Khair, K., G. F. Karakaisis, and E. E. Papadimitriou, Seismic zonation of the Dead Sea transform fault area, *Ann. Geofis.*, *43*, 61–79, 2000.

Kohl, C. P., and K. Nishiizumi, Chemical isolation of quartz for measurement of in-situ-produced cosmogenic nuclides, *Geochim. Cosmochim. Acta*, *56*, 3583–3587, 1992.

Kurushin, R. A., A. Bayasgalan, M. Ölzybat, B. Enhtuvshin, P. Molnar, C. Bayarsayhan, K. W. Hudnut, and J. Lin, The surface rupture of the 1957 Gobi-Altay, Mongolia, Earthquake, in *Geological Society of America Spec. Pap. 320*, 143 pp., 320, 1997.

Lal, D., Cosmic ray labelling of erosion surfaces: In situ nuclide production rates and erosion models, *Earth Planet. Sci. Lett.*, *104*, 424–439, 1991.

Marco, S., M. Stein, A. Agnon, and H. Ron, Long-term earthquake clustering: A 50,000-year paleoseismic record in the Dead Sea Graben, *J. Geophys. Res.*, *101*, 6179–6191, 1996.

McCalpin, J. P., *Paleoseismology*, p. 588, Academic, San Diego, Calif., 1996.

Middleton, R., L. Brown, B. Dezfoulyarjomandy, and J. Klein, On Be-10 standards and the half-life of Be-10, *Nucl. Instrum. Methods Phys. Res.*, *82*, 399–403, 1993.

Molnar, P., and D. Qidong, Faulting associated with large earthquakes and the average rate of deformation in Central and eastern Asia, *J. Geophys. Res.*, *89*, 6203–6227, 1984.

Molnar, P., and P. Tapponnier, Cenozoic Tectonics of Asia: Effects of a continental collision, *Science*, *189*, 419–426, 1975.

Ohno, M., and Y. Hamano, Geomagnetic poles over the past 10,000 years, *Geophys. Res. Lett.*, *19*, 1715–1718, 1992.

Owen, L. A., B. F. Windley, D. W. Cunningham, J. Badamgarav, and D. Dorjnamjaa, Quaternary alluvial fans in the Gobi of southern Mongolia: Evidence for neotectonics and climate change, *J. Quat. Sci.*, *12*, 239–252, 1997.

Owen, L. A., B. Richards, E. J. Rhodes, D. W. Cunningham, B. F. Windley, J. Badamgarav, and D. Dorjnamjaa, Relic permafrost structures in the Gobi of Mongolia: Age and significance, *J. Quat. Sci.*, *13*, 539–547, 1998.

Owen, L. A., D. W. Cunningham, B. W. Richards, E. Rhodes, B. F. Windley, D. Dorjnamjaa, and J. Badamgarav, Timing of formation of forebergs in the northeastern Gobi-Altai, Mongolia: Implications for mountain uplift rates and earthquake recurrence intervals, *J. Geol. Soc. London*, *156*, 457–464, 1999.

Philip, P., and J.-F. Ritz, Gigantic paleolandslide associated with active faulting along the Bogd Fault (Gobi-Altay, Mongolia), *Geology*, *27*, 211–214, 1999.

Prentice, C. S., K. J. Kendrick, K. Berryman, A. Bayasgalan, J. F. Ritz, and J. Q. Spencer, Prehistoric ruptures of the Gurvan Bulag fault, Gobi Altay, Mongolia, *J. Geophys. Res.*, *107*(B12), 2321, doi:10.1029/2001JB000803, 2002.

Raisbeck, G. M., F. Yiou, D. L. Bourlès, J. Lestringuez, and D. Deboffe, Measurements of ^{10}Be and ^{26}Al with a Tandetron AMS facility, *Nucl. Instrum. Methods*, *29*, 22–26, 1987.

Raisbeck, G. M., F. Yiou, D. L. Bourlès, E. T. Brown, D. Deboffle, P. Jouhanneau, J. Lestringuez, and Z. Q. Zhou, The AMS facility at Gif-sur-Yvette: Progress, perturbations and projects, *Nucl. Instrum. Methods*, *92*, 43–46, 1994.

Ritz, J.-F., E. T. Brown, D. L. Bourlès, H. Philip, A. Schlupp, G. M. Raisbeck, F. Yiou, and B. Enkhtuvshin, Slip rates along active faults estimated with cosmic-ray-exposures dates: Application to the Bogd Fault, Gobi-Altay, Mongolia, *Geology*, *23*, 1019–1022, 1995.

Ritz, J.-F., et al., Comparison of uplift rates on 20 and 100 ky timescale along the Gurvan Bulag thrust fault (Gobi-Altay, Mongolia) using cosmic-ray exposure dates, *Eos Trans. AGU*, *78*(17), Spring Meet. Suppl., F46, 1997.

Schlupp, A., Néotectonique de la Mongolie Occidentale analysée à partir de données de terrain, sismologiques et satellitaires, Ph.D. thesis, 172 pp., Univ. Louis Pasteur, Strasbourg, 1996.

Schwartz, D., and K. Coppersmith, Fault behavior and characteristic earthquakes: Examples from the Wasatch and San Andreas faults, *J. Geophys. Res.*, *89*, 5681–5698, 1984.

Sieh, K., M. Stuiver, and D. Brillinger, A more precise chronology of earthquakes produced by the San Andreas fault in southern California, *J. Geophys. Res.*, *94*, 603–623, 1989.

Slemmons, D. B., and C. Depolo, Evaluation of Active Faulting and Associated Hazards, In *Active Tectonics*, pp. 45–62, Natl. Acad. Press, Washington D. C., 1986.

Tapponnier, P., and P. Molnar, Active faulting and Cenozoic tectonics of the Tien Shan, Mongolia and Baykal regions, *J. Geophys. Res.*, *84*, 3425–3459, 1979.

Van der Woerd, J., F. J. Ryerson, P. Tapponnier, Y. Gaudemer, R. Finkel, A. S. Meriaux, M. Caffee, Z. Guoguang, and H. Qunlu, Holocene left-slip rate determined by cosmogenic surface dating on the Xidatan segment of the Kunlun fault (Qinghai, China), *Geology*, *26*, 695–698, 1998.

Xiwei, X., and D. Qidong, Nonlinear characteristic of paleoseimicity in China, *J. Geophys. Res.*, *101*, 6209–6231, 1996.

Yeats, R., and C. Prentice, Introduction to special section: Paleoseismology, *J. Geophys. Res.*, *101*, 5847–5853, 1996.

D. Bourlès, Centre Européen de Recherche et d'Enseignement de Géosciences de l'Environnement (CEREGE), Europole Mediterranéen de l'Arbois, B.P. 80, 13 545 Aix-en-Provence, Cedex 4, France.

E. T. Brown, Large Lakes Observatory, University of Minnesota, Duluth, MN 55812, USA.

S. Carretier, BRGM/ARN3, Av. Claude Guillemin BP 6009, 45000 Orleans, France.

J. Chéry, H. Philip, and J.-F. Ritz, Laboratoire de Géophysique, Tectonique et Sédimentologie, UMR 5573—Université Montpellier II, 4 Place Eugene Bataillon, 34095 Montpellier Cedex 05, France. (ritz@dstu.univ-montp2.fr)

B. Enhtuvshin and P. Galsan, Centre of Informatic and Remote Sensing, Mongolian Academy of Sciences, 210351 Ulaanbaatar, Mongolia.

R. C. Finkel, LLNL, University of California, P.O. Box 808, Livermore, CA 94551-9989, USA.

T. C. Hanks and D. P. Schwartz, U.S. Geological Survey, MS 977, 345 Middlefield Road, Menlo Park, CA 94025, USA.

K. J. Kendrick, U.S. Geological Survey, 525 South Wilson Avenue, Pasadena, CA 91106, USA.

G. Raisbeck and F. Yiou, Centre de Spectrométrie Nucléaire et de Spectrométrie de Masse, IN2P3-CNRS, Bâtiment 108, 91405 Orsay, France.

A. Schlupp, Laboratoire de Télédétection et Risque Sismique, CEA/DIF/DASE/LDG, BP 12, 91680 Bruyères-le-Chatel, France.